Duality of the murine CD8 compartment

Raphaël Genolet[a], Julie Leignadier[a], Magne Østerås[b], Laurent Farinelli[b], Brian J. Stevenson[c], and Immanuel F. Luescher[a,1]

[a]Ludwig Centre for Cancer Research, University of Lausanne, 1066 Epalinges, Switzerland; [b]Fasteris SA, 1228 Plan-les-Ouates, Switzerland; and [c]Vital-IT Group, Swiss Institute of Bioinformatics, 1015 Lausanne, Switzerland

Edited* by K. Christopher Garcia, Stanford University, Stanford, CA, and approved January 31, 2014 (received for review September 21, 2013)

CD8αβ plays crucial roles in the thymic selection, differentiation, and activation of some, but not all, CD8$^+$ T cells, whereas CD8αα does not. To investigate these roles, we produced mice that expressed transgene P14 T-cell receptor β (TCRβ) chain and CD8β or did not (WT and KO mice, respectively). The primary CD8$^+$ T-cell response to acute lymphocytic choriomeningitis virus (LCMV) infection was predominantly D^b/GP33 specific and CD8 independent in KO mice and was mostly CD8 dependent in WT mice. Cytotoxic T lymphocytes (CTL) from KO mice failed to mobilize intracellular Ca^{2+} and to kill via perforin/granzyme. Their strong Fas/FasL-mediated cytotoxicity and IFN-γ response were signaled via a Ca^{2+}-independent, PI3K-dependent pathway. This was also true for 15–20% of CD8-independent CTL found in WT mice. Conversely, the perforin/granzyme-mediated killing and IFN-γ response of CD8-dependent CTL were signaled via a Ca^{2+}, p56^{lck}, and nuclear factor of activated T cells-dependent pathway. Deep sequencing of millions of TCRα chain transcripts revealed that the TCR repertoires of preimmune CD8$^+$ T cells were highly diverse, but those of LCMV D^b/GP33-specific CTL, especially from KO mice, were narrow. The immune repertoires exhibited biased use of Vα segments that encoded different complementary-determining region 1α (CDR1α) and CDR2α sequences. We suggest that TCR from WT CD8-independent T cells may engage MHC–peptide complexes in a manner unfavorable for efficient CD8 engagement and Ca^{2+} signaling but permissive for Ca^{2+}-independent, PI3K-dependent signaling. This duality of the CD8 compartment may provide organisms with broader protective immunity.

T-cell receptor α and β–positive (TCRαβ$^+$) CD8$^+$ T cells and cytotoxic T lymphocytes (CTL) play a crucial role in the elimination of pathogen-infected and transformed cells (1, 2). CTL are activated upon engagement of their TCR with cognate peptide–MHC I complexes (pMHC) on antigen-presenting or target cells (3, 4). CD8αβ plays important roles in thymic selection, CD8$^+$ T-cell differentiation, and antigen recognition (1, 5, 6). CD8 also can be expressed as a CD8αα homodimer, e.g., on intraepithelial lymphocytes, natural killer T cells, and TCRγδ$^+$ T cells (7). Although CD8αα and CD8αβ bind similarly to MHC class I molecules (8), CD8β endows CD8 with coreceptor functions. Indeed, CD8αβ, but not CD8αα, associates with TCR/CD3, strengthens pMHC binding (3–5, 9, 10), and promotes CD8 association with lipid rafts and p56^{lck} (lymphocyte-specific tyrosine kinase, lck) and hence TCR signaling via lck-mediated phosphorylation of CD3 ITAMs, followed by recruitment and activation of Zeta-chain–associated protein kinase 70 (ZAP-70), phosphorylation of Linker for activation of T cells (LAT), and diverse downstream signaling cascades, including activation of phospholipase C-γ (PLCγ), mobilization of intracellular Ca^{2+}, and translocation of the transcription factor, Nuclear factor of activated T cells (NFAT) (3–5,9–11). CD8β-KO mice have two- to-threefold lower numbers of CD8$^+$ T cells, showing that CD8β plays an important but not essential role in the thymic selection of CD8$^+$ T cells (5, 12, 13). Nevertheless, CD8β- (and CD8α-) KO mice efficiently clear acute viral infections [e.g., lymphocytic choriomeningitis virus (LCMV), influenza, or vesicular stomatitis virus (2, 12, 14)]. Their CTL avidly kill, produce cytokines, and are CD8 independent. A study using OT I TCR-transgenic mice indicated that, in the absence of CD8, thymic selection relied on higher-affinity ligands (15).

It has been reported that CD8$^+$ T cells from CD8β- (and CD8α-) KO mice express higher-affinity TCR that allow recognition of infected cells in the absence of the CD8αβ coreceptor (14, 16). However, other studies claim that CD8 dependence is related to TCR sequences and that CD8-independent T cells can express low-affinity TCR (2, 17–20). This latter view is supported by the observations that CD8 independence or dependence can be conveyed by TCR gene transfer (18, 20) and that the TCR repertoires of CD8-independent, virus-specific CTL from CD8β- or CD8α-KO mice are different from TCR repertoires of such CTL from normal mice (2, 14, 17).

CD8$^+$ (and CD4$^+$) T cells are generated by a multistep process in the thymus. During the last CD4$^-$, CD8$^-$ stage, thymocytes undergo TCRβ variable, diversity and joining (VDJ) recombination, and rearranged TCRβ chains must pair with the pre-TCRα chain to warrant continuation of development (1, 5–7). On CD4$^+$, CD8$^+$ double-positive thymocytes, TCRα V, J recombination is initiated, which starts with primary rearrangements that are focused on proximal Vα (T-cell alpha variable, TRAV) and Jα (TRAJ) gene segments and proceeds independently on both alleles (1, 21). Unless primary rearrangements yield a selecting TCR, up to five secondary rearrangements can take place, which have been reported to proceed in a sequential coordinated fashion, implying that only of fraction of all possible TRAV–TRAJ rearrangements can be realized (21). At variance with this process, the sequencing of millions of TCRα chain transcripts from CD8$^+$ T cells from C57BL/6 (B6) mice revealed that the repertoire is much larger than had been anticipated and exhibits no "forbidden" TRAV–TRAJ rearrangements (22).

Significance

CD8αβ is expressed on CD8$^+$ T cells and can govern their thymic selection, differentiation, and effector functions by inducing Ca^{2+} and nuclear factor of activated T cells (NFAT)-dependent signaling. Conversely, we showed that CD8-independent T cells are signaled in a Ca^{2+}-independent, PI3K-dependent manner. By assessing the physical and functional affinities, signaling, and TCR repertoires of CD8-dependent and -independent T cells, we uncovered correlates between effector functions, their triggering, and the TCR repertoires. We suggest that the docking orientations of TCR–MHC complexes may influence CD8$^+$ T-cell signaling and hence their functions. Together, these data argue that signaling events rather than affinity determine CD8 dependency and that the duality of the CD8 compartment may provide the organisms with broader protective immunity.

Author contributions: R.G., J.L., and I.F.L. designed research; R.G., J.L., M.Ø., and L.F. performed research; R.G., J.L., and B.J.S. analyzed data; and R.G., B.J.S., and I.F.L. wrote the paper.

The authors declare no conflict of interest.

*This Direct Submission article had a prearranged editor.

[1]To whom correspondence should be addressed. E-mail: immanuel.luescher@unil.ch.

This article contains supporting information online at www.pnas.org/lookup/suppl/doi:10.1073/pnas.1317847111/-/DCSupplemental.

A xeno-reactive TCR that has been selected in the absence of CD8 has been shown to bind its pMHC complex in a noncanonical diagonal docking orientation that precludes CD8αβ coengagement (23). Moreover, in the 3D structure a large number of TCR–pMHC I complexes revealed that most TCR engage their pMHC in a canonical diagonal mode, but other docking orientations do exist (24–26). Given the structure of CD8αβ and its pMHC binding mode, these other docking orientations do not allow coordinate binding of CD8 to TCR-associated pMHC. (8, 23). The coordinate binding provides proximity of CD8-associated lck to TCR-associated CD3, explaining why TCR engaging pMHC in noncanonical orientations exhibit ablated lck/ZAP70/LAT/NFAT signaling (23–27).

Here we investigated why IFN-γ and cytolytic functions of some but not other $CD8^+$ T cells depend on coreceptors. We used B6 mice that expressed the TCRβ chain of the LCMV D^b/GP33 tetramer-specific P14 TCR and CD8β (WT mice) or did not (KO mice) and examined their LCMV-induced CTL responses. Because of allelic exclusion, all $TCR\alpha\beta^+$ T cells derived from these mice express the P14 TCRβ chain (1). Most CTL from WT mice avidly produced IFN-γ and killed via perforin/granzyme upon Ca^{2+}- and NFAT-dependent signaling. Conversely, CTL from KO mice efficiently produced IFN-γ and killed via Fas/FasL upon Ca^{2+}-independent and PI3K-dependent signaling. A minor fraction of CTL from WT mice exhibited the same CD8-independent signaling. Analysis of the TCR repertoires of LCMV-specific CTL revealed, in addition to significant overlaps, exclusive or preferential use of TRAV gene segments that encoded different CDR1α and CDR2α sequences. Because TCR dock onto MHC molecules primarily via their CDR1 and CDR2 loops, we speculate that TCR from CD8-independent CTL may engage pMHC in orientations that preclude efficient CD8 cosignaling but allow triggering via an alternative Ca^{2+}-independent, PI3K-dependent pathway.

Results

CTL from WT and KO Mice Kill by Different Mechanisms. To investigate the impact of CD8β on $CD8^+$ T-cell function, we generated mice expressing P14 TCRβ chain and expressing or not CD8β (WT and KO mice, respectively). The KO mice had nearly twofold fewer splenic $CD8^+$ T cells and modestly more $CD4^+$ T cells (Fig. S1 *A* and *B*). Eight days after acute LCMV infection the number of $CD8^+$ splenocytes increased by more than twofold in WT mice, slightly more than in KO mice (Fig. S1 *C* and *D*). There were few differences in the expression of CD44, CD25, and CD127 on $CD8^+$ T cells from naive or LCMV-immune WT and KO mice, except that CD5 expression was increased on cells from WT mice and CD62L expression was increased on cells from KO mice (Fig. S1*E*). Approximately 56% of the splenocytes from LCMV-immune WT mice were $CD8^+$ D^b/GP33 tetramer positive, but less than 1% were D^b/NP396, D^b/GP276, or K^b/205 tetramer positive (Fig. 1*A*). Of the splenocytes cells from LCMV-immune KO mice, 8.8% were $CD8^+$ D^b/GP33 tetramer positive, and 1.7–3.4% positive for the other tetramers. $CD4^+$ splenocytes from LCMV-immune mice were poorly stained by all tetramers (0.08–0.43% and 0.3–1.2% for WT and KO mice, respectively) (Fig. 1*B*).

We performed cytolytic experiments with CTL derived from LCMV-immune WT and KO mice using ^{51}Cr-labeled P815/D^b target cells pulsed with graded concentrations of WT GP33 or variant peptides. Efficient killing was observed for both CTL with the WT peptide, but substantial differences were observed with the GP33 variant peptides (Figs. 1 *C* and *D*). For example the peptide containing A in place of Y36 (Y36A) was recognized efficiently by CTL from WT mice but was recognized very poorly by CTL from KO mice: A 1,155-fold higher peptide concentration was required for half-maximal lysis, and the maximal lysis was nearly threefold lower. To investigate whether different cytolytic mechanisms cause the great differences in target cell killing, CTL from WT or KO mice were incubated with P815/D^b cells pulsed with GP33 peptide, and their CD107a (Lamp-1) expression was assessed by flow cytometry. The CTL from WT, but not from KO, mice exhibited strong CD107a expression, indicating that CTL from KO mice have severely impaired degranulation, i.e., defective perforin/granzyme-mediated cytotoxicity (28). Moreover, CTL from WT mice exhibited high and stable intracellular Ca^{2+} mobilization upon incubation with P815/D^b cells pulsed with GP33 peptide; the CTL from KO mice did not (Fig. 1*G*). The intracellular Ca^{2+} mobilization in the CTL from KO mice was clearly less intense than that in the CTL from WT mice, especially at elevated peptide concentrations; however, there was not as great a difference in the frequencies of Ca^2-fluxing cells (Fig. S2). The requirement of strong and sustained Ca^{2+} mobilization for CTL degranulation (29) explains why CTL from KO mice have ablated perforin/granzyme-mediated killing.

Because CTL also can kill via FasL-mediated crosslinking of Fas on other cells (28, 30), we assessed the FasL expression on cells from WT and KO mice. Preimmune $CD8^+$ T cells from KO mice expressed modestly higher FasL levels on the cell surface than did cells from WT mice, but their intracellular FasL expression was more than 40-fold higher (Fig. 1*F*). Conversely, CTL from KO mice exhibited three times higher FasL surface expression than cells from WT mice, but their intracellular FasL expression was only modestly higher. As assessed by ^{51}Cr-release experiments, the killing by CTL from WT mice was inhibited strongly by concanamycin A (CMA), an inhibitor of perforin/granzyme-mediated cytotoxicity (31). Conversely, the killing by CTL from KO mice was not affected by CMA but was strongly inhibited by anti-FasL antibody, which had little effect on the killing by CTL from WT mice (Fig. 1*H*). These results indicate that CTL from WT mice kill mainly via perforin/granzyme, but those from KO mice kill via Fas/FasL-mediated cytotoxicity.

CTL from WT and KO Mice Exhibit Different Tetramer Binding and IFN-γ Signaling. To investigate the pMHC-binding properties of CTL from WT and KO mice, we performed D^b/GP33 tetramer binding. Maximal tetramer binding reached slightly higher levels on CTL from WT mice than on cells from KO mice (100% versus 80%) but was modestly less avid (Fig. 2 *A* and *B*). Scatchard analysis of multiple binding experiments indicated dissociation constants (K_d) of 4.8 and 4.0 nM and maximal binding (B_{MAX}) of 104 and 83, respectively. The same experiment performed with CD8-binding–deficient $D^b_{226/227}$/GP33 tetramer exhibited reduced binding on CTL from WT mice (K_d 10.8 nM; B_{MAX} 78.5) but not on CTL from KO mice (K_d 6.2 nM; B_{MAX} 85.6). The differences in maximal binding were not accounted for by differences in TCR or CD8 expression on the cells, because CTL from KO mice expressed 1.68-fold more TCR and 1.2-fold less CD8α.

As assessed by intracellular cytokine staining, an efficient IFN-γ response was observed in CTL from LCMV-immune WT mice (half-maximal response at 0.07 nM GP33 peptide) (Fig. 2 *C* and *D*). The IFN-γ response was lower on cells from KO mice (~75% of cells responding; half-maximal response at 0.21 nM GP33 peptide). The IFN-γ response of cells from WT, but not from KO, mice was reduced substantially in the presence of blocking anti-CD8α mAb. Similar results were obtained when the TNF-α response was measured in the same way (Fig. 2*D*).

We next examined the susceptibility of the IFN-γ responses of CTL from WT and KO mice to different enzyme inhibitors. Cyclosporin A (CsA), an inhibitor of calcineurin and NFAT (32), profoundly inhibited the IFN-γ response of CTL from WT, but not from KO, mice (Fig. 2*E*). Conversely the PI3K inhibitors Wortmannin and Ly294002 strongly inhibited the IFN-γ response of CTL from KO mice but had little effect on the response of CTL from WT mice. Wortmannin and CsA combined inhibited ~95% of the IFN-γ response of CTL from WT mice but only ~80% of the response of CTL from KO mice. Thus, CTL from both WT and KO mice mount strong IFN-γ responses, but different pathways

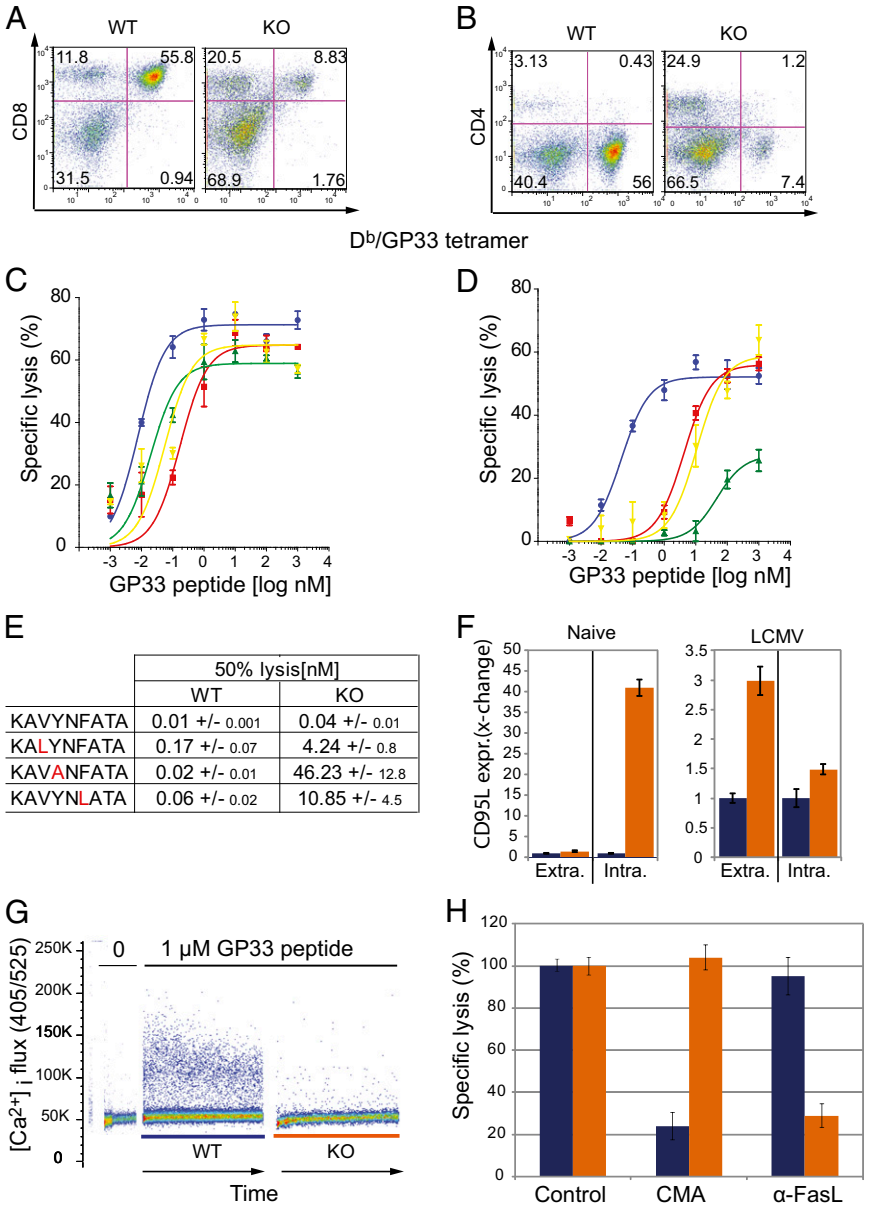

Fig. 1. Characterization of LCMV GP33-specific CTL and their cytolytic T-cell responses. (*A* and *B*) Eight days after LCMV infection CD8$^+$ (*A*) and CD4$^+$ (*B*) splenocytes from WT and KO mice were stained with D^b/GP33$^+$ tetramers and anti-CD8 or anti-CD4 antibody and were analyzed by flow cytometry. The numbers indicate the percentage of cells in the different quadrants. (*C* and *D*) CTL from WT (*C*) or KO (*D*) mice were incubated with ^{51}Cr-labeled P815/D^b cells prepulsed with the indicated concentrations of WT GP33 (blue) or the variant peptides V35L (red), Y36A (green), or F38L (yellow), and the specific lysis was determined. Mean values and SD were calculated from two experiments. (*E*) The peptide concentrations (in nanomolars) for half-maximal lysis. (*F*) The mean fluorescence intensity (MFI) of FasL surface (Extra) or intracellular (Intra) staining was assessed by flow cytometry on CD8$^+$ T cells from preimmune (Naive) or LCMV-immune (LCMV) WT (blue bars) or KO (orange bars) mice. The value observed on CTL from WT mice was set as one. Mean values and SD were calculated from two experiments. (*G*) D^b/GP33 tetramer-sorted Indo-1–labeled cells from LCMV-immune WT or KO mice were incubated with P815/D^b cells pulsed or not pulsed with the indicated concentrations of GP33 peptide. Ca^{2+} mobilization was assessed by flow cytometric recording of the 405/525 nm fluorescence ratio (*y*-axis) over 5 min (*x*-axis). (*H*) ^{51}Cr-release experiment as described in *A* using as targets P815/D^b cells pulsed with 1 μM GP33 peptide. CTL from WT (blue bars) or KO (orange bars) mice were incubated in the absence (control) or presence of CMA or anti-FasL antibody (FasL). Mean values and SD were calculated from two experiments.

signal these responses. Together, these data argue that signaling events rather than affinity determine CD8 dependency.

TCR Repertoires of CD8$^+$ T Cells from WT and KO Mice. The TCRα chain repertoire of CD8$^+$ T cells from naive WT mice was remarkably diverse, exhibiting 91.1% of all possible TRAV–TRAJ rearrangements (Figs. S3 *A* and *C* and S4). The TRAV–TRAJ recombination frequency map indicated that the three most proximal TRAV segments preferentially recombined with proximal TRAJ gene segments; however, all other TRAV segments recombined with nearly every TRAJ segment. The recombination frequencies varied with the TRAV gene use, ranging from zero (e.g., TRAV14N-3, TRAV14N-2) to low (e.g., TRAV6-7, TRAV12-2) to high (e.g., TRAV 9-1, TRAV4N-4). The repertoire of CD8$^+$ T cells from naive KO mice comprised 85.2% of all possible TRAV–TRAJ recombinants (Fig. S3 *B* and *C*), and their frequencies again depended on TRAV segment use; it was zero for the same TRAV segments, arguing that the corresponding

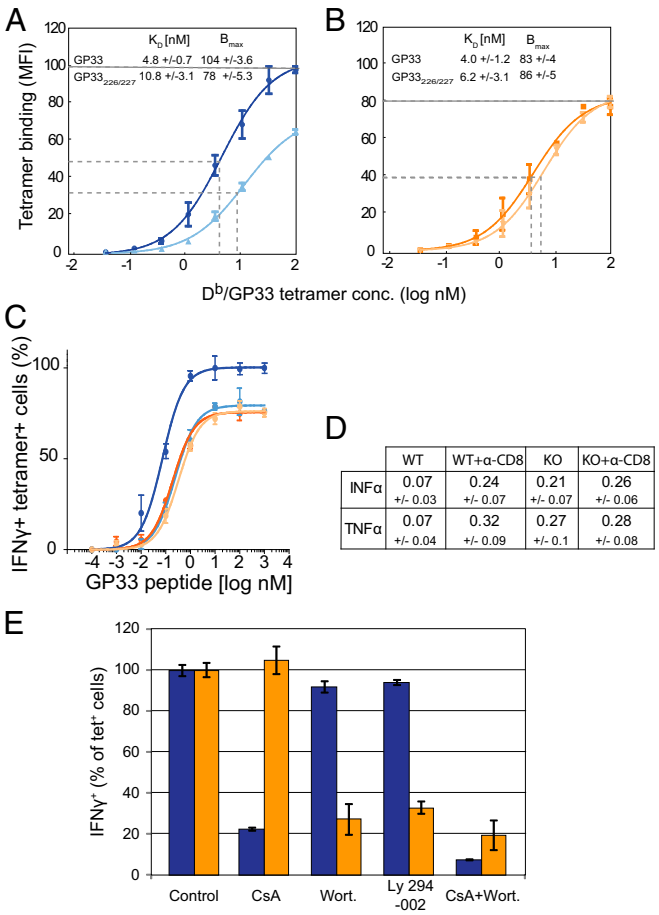

Fig. 2. CTL from WT and KO mice exhibit divergent tetramer binding and IFN-γ responses. (*A* and *B*) $CD8^+$ T cells from LCMV-immune WT (*A*) or KO (*B*) mice were incubated with graded concentrations of D^b/GP33 (dark traces) or $D^b_{266/227}$/GP33 tetramer (light traces), and cell-associated fluorescence was assessed by flow cytometry. The level of tetramer binding measured on CTL from WT mice was set as 100%. The gray dashed lines indicate the GP33 peptide concentrations for maximal and half-maximal binding, respectively. The inserted numbers indicate dissociation constants (K_d) and maximal binding values (B_{max}) as determined by Scatchard analysis. Mean values and SD were calculated from three experiments. (*C*) CTL from WT (blue traces) or KO (orange traces) mice were incubated in the absence (dark traces) or presence (light traces) of blocking anti-CD8α mAb 53.6.72 with graded concentrations of GP33 peptide for 6 h, were stained with D^b/GP33 tetramer and then were stained intracellularly for IFN-γ, and were analyzed by flow cytometry. Maximal counts of WT D^b/GP33 tetramer-positive IFN-γ^+ cells represent 100%. (*D*) Compilation of the GP33 peptide concentrations (in nanomolars) for which half-maximal INFγ or TNF-α (assessed as in *C*) responses were observed. Mean values and SD were calculated from three experiments. (*E*) CTL from WT (blue bars) or KO (orange bars) mice were incubated in the absence (control) or presence of Wortmannin (Wort), LY294002, and/or CsA with GP33 peptide-pulsed P815/D^b cells. After 6 h the intracellular IFN-γ expression of D^b/GP33 tetramer-positive cells was assessed by flow cytometry. The highest value of tetramer-positive IFN-γ^+ cells represents 100%. Mean values and SD were calculated from two experiments.

TCRα chains failed to pair efficiently with the transgene P14 TCRβ chain or were selected in other lineages in the thymus (1, 7, 21, 33). The frequency maps for the CDR3α sequence were similar to those of the TRAV–TRAJ rearrangements, arguing that the junctional diversity depends on the probability of TRAV–TRAJ recombination (Fig. S3 *E* and *F*). Remarkably, most CDR3α sequences were different on cells from WT and KO mice, although many were expressed at low frequencies (Fig. S3*D*).

The TCR repertoire of D^b/GP33 tetramer-sorted CTL from LCMV-immune WT mice comprised 65% of all possible TRAV–TRAJ gene recombinants (Fig. 3 *A* and *C*), and the TRAV–TRAJ recombination frequency plot resembled that of preimmune cells (Fig. 3*A* and Figs. S3*A* and S4). In contrast, CTL from KO mice exhibited greatly reduced TRAV–TRAJ recombinants, as compared with preimmune $CD8^+$ T cells, and a marked overexpression of the TRAJ48 segment containing recombinants (Fig. 3 *B* and *C* and Figs. S3*B* and S5*B*). The distributions of CDR3α sequences resembled those of the TRAV–TRAJ rearrangements (Fig. 3 *A*, *B*, *E*, and *F*). The majority of the CDR3α sequences were found either on WT or KO CTL. However, their frequencies were considerably smaller, indicating that shared sequences were expressed more frequently than unique ones (Fig. 3*D* and Fig. S5).

CDR3α Sequence Analyses of D^b/GP33-Specific CTL. The TRAV14D-1–TRAJ48 recombination was overrepresented in the TCR repertoires of D^b/GP33-specific CTL from WT and especially from KO mice (Fig. S5*A*). More than 50% of the corresponding CDR3α sequences were found only on CTL from WT or KO mice; however, except for the 12-aa P14 TCRα chain CDR3α sequence (CAALYGNEKITF) that was overrepresented (Figs. S5*B* and S6*A*), most of these sequences were expressed at low frequencies. Positional amino acid scoring of the dominant 12-residue-long CDR3α sequences found on CTL from KO, but not from WT, mice revealed a strong overrepresentation of leucine (L) in position four (Fig. S6*B*). Analysis of the CDR3α sequences of the TRAJ48 segment containing recombinants showed that most sequences were 12 aa long, but many sequences on CTL from WT mice were 13 aa long, and some sequenced on CTL from KO mice were 14 residues long (Fig. S6*C*). Positional amino acid frequency analysis again showed a strong preference for leucine in position four of 12-residue-long CDR3α sequences on CTL from KO, but not from WT, mice (Fig. S6*D*). The 14-residue-long CDR3α sequences observed on CTL from KO mice c preferentially contained proline in position 5, which was not the case for sequences found on CTL from WT mice. The CDR3α sequences of all D^b/GP33-specific CTL from WT mice showed a nearly Gaussian length distribution, with a maximum length of 15 residues, whereas those sequences on CTL from KO mice were preferentially 12, 14, and 18 residues long (Fig. S6*E*). It is noteworthy that because gene rearrangements in the TCRα chain can occur on both chromosomes, $CD8^+$ T cells can express two TCRα chains; therefore the TCRα chain repertoire determined by our method appears more diverse than it is. TCR repertoire analysis based on sequencing the TCRα-chain transcripts of single, virus-specific mouse CTL indicated that ~25% of the cells have two TCRα transcripts, about 10% of which are in frame (34). Because out-of frame sequences were disregarded in our analysis, the diversity in our TCR repertoire analysis appears to be about 10% higher than is actually the case.

The TCR Repertoires of CTL from WT and KO Mice Are Skewed. The TCR repertoires of D^b/GP33-specific CTL from WT and KO mice overlapped but also diverged (Fig. 3 and Figs. S5 and S6). For example, the frequencies of certain TRAV–TRAJ recombinants varied up to several thousand-fold between the two sets (Fig. 4 *A* and *B*). Moreover, some TRAV–TRAJ recombinants were observed only on CTL from WT or KO mice (Fig. 4 *C* and *D*). By calculating for each TRAV segment the percentage of recombinants found in the WT repertoire and ranking these percentages in rising order, we observed a skewed TRAV segment use; that is, some TRAV segments were found exclusively or preferentially in the repertoire of CTL from WT or KO mice (Fig. 4*E* and Fig. S7). The position of these TRAV genes in the TCRα/δ locus was apparently random (Figs. S4 and S7).

We selected the eight most biased WT or KO TRAV gene segments (Fig. S7) and compared their CDR1α and CDR2α sequences (Fig. 5*A*). The CDR1α sequences were, on average, longer than the CDR2α sequences and were more diverse in length.

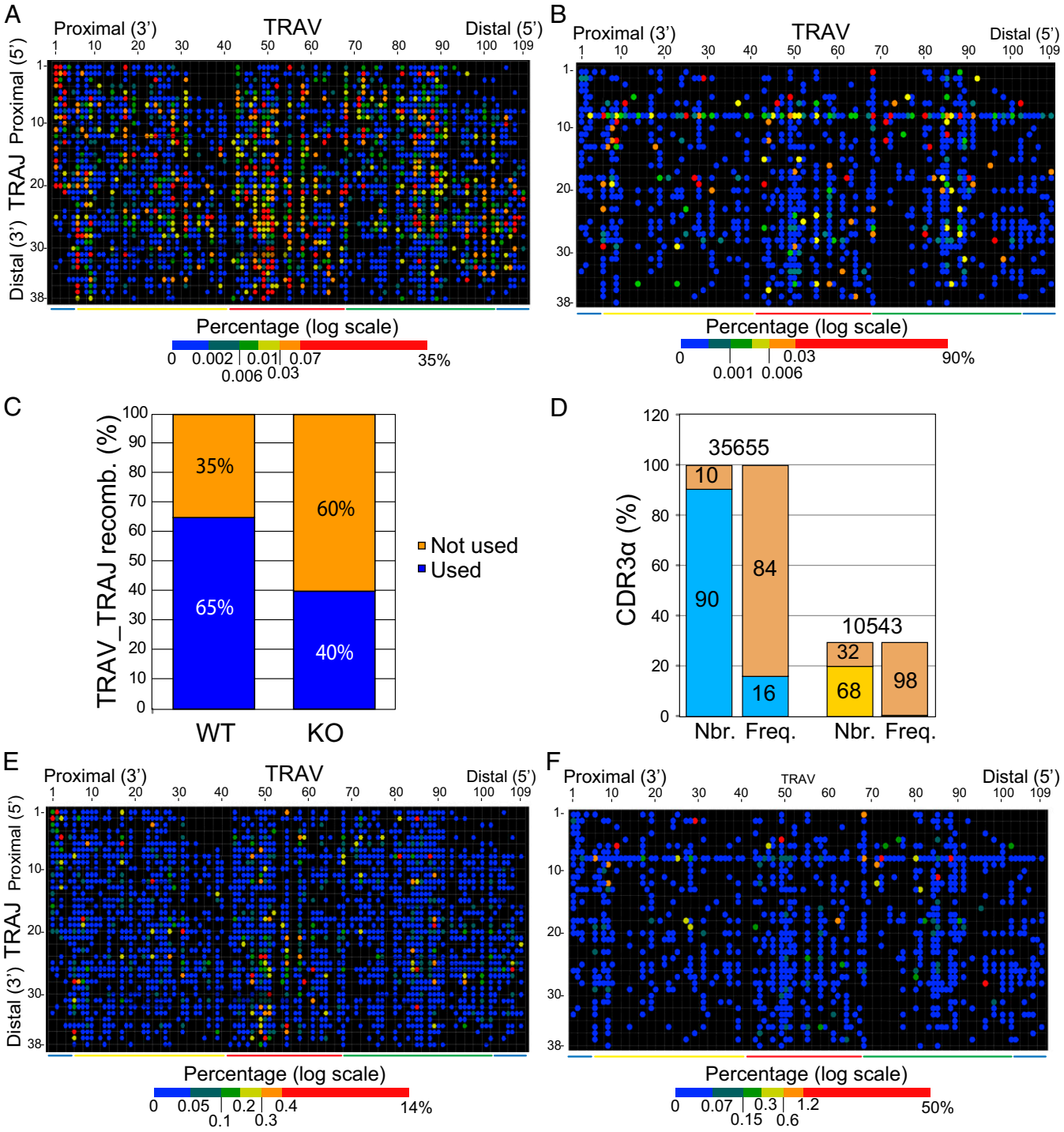

Fig. 3. TCRα chain repertoires of D^b/GP33$^+$-specific CD8$^+$ CTL. (*A* and *B*) Transcripts of D^b/GP33 tetramer-sorted splenocytes 8 d after LCMV infection from WT (*A*) or KO (*B*) mice were sequenced, and the number of TRAV–TRAJ recombinations was plotted versus the functional TRAV (*x*-axis) and TRAJ gene segments (*y*-axis) listed in order of their chromosomal locations (Fig. S4). The frequencies of the recombinants are indicated by the color coding shown in the underlying bar. (*C*) The number of TRAV/TRAJ recombinants found on cells from WT and KO mice are shown as blue bars representing the percentage of all possible rearrangements (4,142). (*D*) The number and frequency of CDR3α sequences observed on cells from WT (blue bars), KO (orange bar), or both WT and KO (brown bars) mice are represented as the percentage of all CDR3α sequences. The digits indicate the numbers of CDR3α sequences. (*E* and *F*) The number of CDR3α sequences for each TRAV–TRAJ rearrangement observed on cells from WT (*E*) or KO (*F*) mice are plotted against the TRAV (*x*-axis) and the TRAJ (*y*-axis) gene segments listed according to their chromosomal locations. The frequencies of CDR3α sequences are indicated by the color coding shown in the underlying bar.

Comparison of the two sets of CDR1α and CDR2α sequences revealed that CDR1α sequences preferentially contained polar residues in positions 4 and 8 in the WT, but not the KO, group and proline or tyrosine in position 10 in the WT, but not in the KO, group. Also, the CDR2α sequences from the KO group contained more hydrophobic residues, namely in positions 3 and 5. The

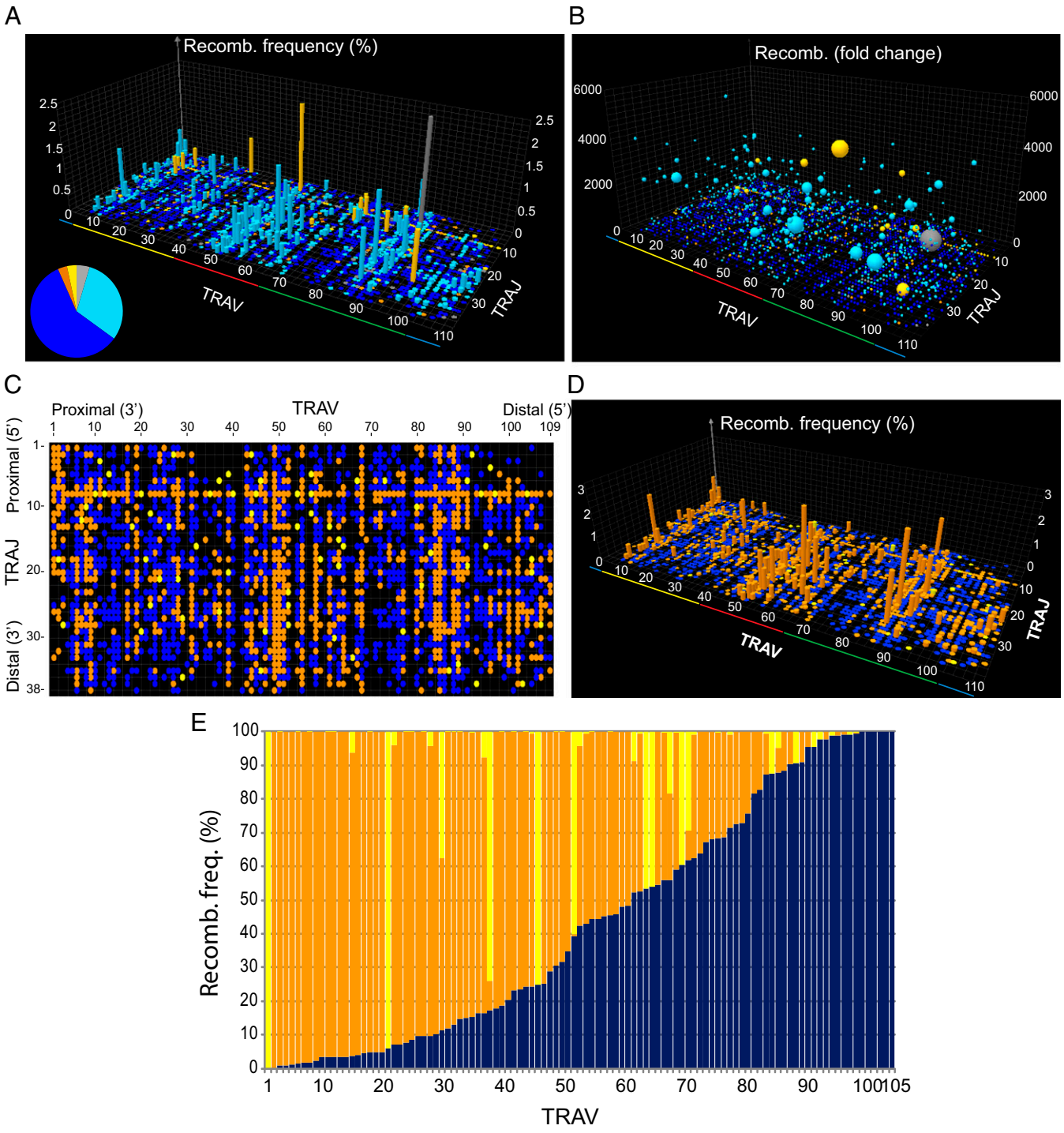

Fig. 4. Sidedness of the immune TCR repertoires. (*A*) The frequency of TRAV–TRAJ recombinants (*z*-axis; % of total) expressed more than twofold more frequently on D^b/GP33 tetramer-positive CTL from WT mice (light blue) than on CTL from KO mice (orange) or expressed exclusively on the cells from WT (dark blue bars) or KO (yellow bars) mice are plotted against the TRAV (*x*-axis) and TRAJ (*y*-axis) segments, listed in order of their chromosomal locations (Fig. S4). The gray bars represent recombinants with greater than twofold changes, and the pie chart shows the percentages of TRAV–TRAJ rearrangements observed for the different groups. (*B*) The fold changes in recombination frequencies (*z*-axis; fold change) from *A* are plotted as spheres against the TRAV and TRAJ gene segments; except for the gray sphere, the size of the spheres represents the frequency of sequences. (*C*) The TRAV–TRAJ rearrangements of D^b/GP33-specific CTL are represented in a 2D graph in which functional TRAV (*x*-axis) and TRAJ (*y*-axis) genes are plotted according to their chromosomal location. Rearrangements uniquely found on CTL from WT mice are represented in dark blue; rearrangements observed only on cells from KO mice are in yellow; and rearrangements common to cells from both WT and KO mice are in orange. (*D*) 3D plot of *C* in which the *z*-axis represents the frequency of the recombinants (percentage of total), the *x*-axis represents the TRAV gene segments, and the *y*-axis represents the TRAJ gene segments. The abundant TRAV14D-1 $(88)^4$–TRAJ48 $(8)^4$ recombination is omitted. (*E*) For each TRAV segment the frequency of recombinants observed only on CTL from WT (blue) or KO (yellow) mice or on both (orange) is represented as a percentage (*y*-axis) and plotted against the TRAV segments (*x*-axis) listed in order of increasing percentages of WT-unique recombination.

hydropathy of the CDR1α and CDR2α sequences [calculated according to Hopp and Woods (35)] was higher in the KO than in the WT group (Fig. 5*B*). The isoelectric point of the CDR1α sequences was nearly two units higher in the KO than in the WT group and was remarkably high in the CDR2α sequences of both groups because of high lysine content (Fig. 5 *A* and *B*).

In the canonical docking mode, αβTCR engages pMHC I complexes in a diagonal orientation, so that the TRAV-encoded CDR1α and CDR2α loops interact with the α2-helix of the MHC molecule and with the hypervariable CDR3α loop (the N-terminal portion of the MHC bound peptide) (24–26). Given the substantial differences between the WT and KO CDR1 and CDR2 sequences, we propose that TCR uniquely or preferentially expressed on CTL from KO mice may engage pMHC in a noncanonical docking mode(s) (Fig. 5*C*). This hypothesis is consistent with structural data indicating that CD8 binds to pMHC in a defined orientation (8) and that a CD8-independent TCR engages its pMHC complex in a noncanonical TCR–pMHC docking mode that precludes CD8 coengagement and hence recruitment of CD8-associated lck to TCR/CD3 (23). We suggest that such TCR permit efficient PI3K signaling instead.

We examined whether LCMV-infected WT mice produce CTL that exhibit the same activation profile as the CD8-independent CTL from LCMV-immune KO mice. Upon stimulation of CTL from LCMV-immune WT mice in the presence of Wortmannin, about 15.6% of the D^b/GP33 tetramer-positive cells were IFN-γ^-, and 82.8% were IFN-γ^+ (Fig. 5*D*). Without Wortmannin pretreatment, 2.1 ± 0.2 of D^b/GP33 tetramer-positive cells were IFN-γ^-. Incubation of the sorted IFN-γ^- cells (15.6%) with GP33 peptide-pulsed P815/D^b cells resulted in an IFN-γ response that was not affected by CsA but was strongly inhibited by Wortmannin (Fig. 5*E*). We extended these experiments by including GP33 peptide-presenting cells and P815 cells expressing CD8-binding–deficient $D^b_{226/227}$. Although CsA had no significant effect, Wortmannin markedly inhibited the IFN-γ response, regardless what antigen-presenting cells were used (Fig. S8). On the other hand, the IFN-γ response of the sorted IFN-γ^+ cells (82.6%) was severely inhibited by CsA but was not affected by Wortmannin (Fig. 5*E*). Moreover, we examined the same IFN-γ^+ and IFN-γ^-, tetramer-positive T cells for D^b/GP33 tetramer binding and found a binding difference comparable to the one observed between CTL from WT and KO mice (Fig. 2 *A* and *B* and Fig. S9). Taken together, these results indicate that a minor fraction of the CTL produced by LCVM-immune WT mice exhibit the same CD8-independent activation requirements and tetramer binding as CTL derived from KO mice.

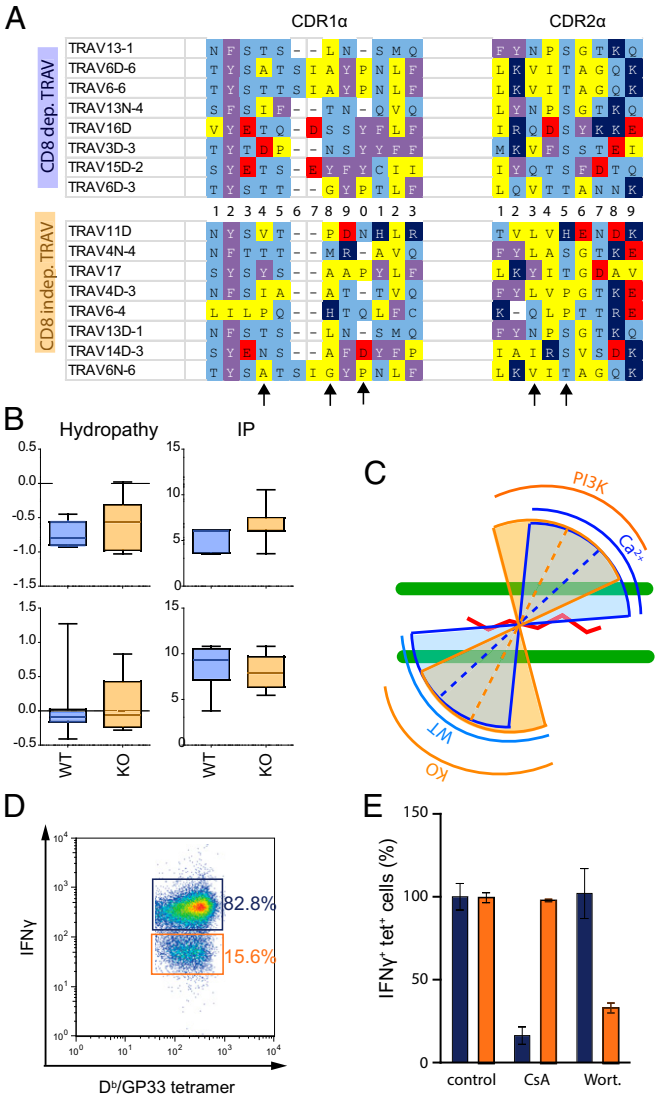

Fig. 5. Proposed TCR repertoire, structure, and CD8$^+$ T-cell signaling correlation. (*A*) The CDR1α and CDR2α sequences of the eight TRAV segments exclusively or preferentially used in the TCR repertoires of CTL from WT or KO mice are shown. Amino acids are color coded (acidic, red; basic, dark blue; aliphatic, yellow; aromatic, purple; polar, light blue); the numbers indicate the residue position, and the arrows indicate differences between CTL from WT and KO mice. (*B*) The hydropathy (34) and isoelectric point (IP) for the CDR1α and CDR2α sequences are represented by boxes indicating the 10th to 90th percentiles and whiskers indicating the maximal and minimal outliers; horizontal lines indicate median values. (*C*) Cartoon representation of the TCR docking onto the MHC–peptide complex (MHC is shown in green and the peptide in red) and the TCR footprint of a canonical (CD8-dependent, Ca^{2+}) binding (blue) and of a noncanonical (CD8-independent, PI3K-dependent) binding (orange). The dashed lines indicate the axes across the CDR3α and CDR3β loops. (*D*) CD8$^+$ T cells from WT mice 8 d post LCMV infection were incubated with Wortmannin and P815/D^b cells pulsed with GP33 peptide, stained with reversible D^b/GP33 tetramer and anti–IFN-γ antibody, and FACS sorted in a tetramer-positive, IFN-γ^+ (blue gate) and a tetramer-positive, IFN-γ^- (orange gate) population. (*E*) The sorted cells were incubated for 4 h with P815/D^b cells, prepulsed with 1 μM GP33 peptide in the absence (–) or presence (+) of CsA or Wortmannin (Wort). The IFN-γ^+, tetramer-positive cells were determined by flow cytometry and are represented as a percentage of the values observed in the absence of inhibitors. Mean values and SD were calculated from two experiments. Colors in the bar graph are as in in *D*.

Discussion

An important observation from the present study was that the intracellular Ca^{2+} mobilization wa significantly less intense in the CTL from KO mice than in the CTL from WT mice (Fig. 1*G* and Fig. S2). CTL degranulation requires high and sustained cytoplasmic Ca^{2+} concentrations, and this requirement explains the dramatically reduced granzyme/perforin-mediated cytotoxicity of CTL from KO mice (Fig. 1) (29). CD8β has been shown to increase substantially the association of CD8 with lck, LAT, TCR/CD3, and lipid rafts, thereby promoting CD3 phosphorylation by coreceptor-associated lck, followed by recruitment and activation of ZAP-70 and diverse downstream signaling cascades, including activation of PLCγ and strong mobilization of intracellular Ca^{2+} via calcium release-activated calcium (CRAC) channels (3-5, 9, 10, 36, 37). Strong Ca^{2+} signaling is crucial to the activation of NFAT, a transcription factor critically involved in CTL triggering of cytokine responses and perforin/granzyme mediated killing (29, 32, 38). The intensity of intracellular Ca^{2+} mobilization and hence NFAT activity was substantially reduced In CTL from CD8β (and CD8α) KO mice, but these cells proliferated upon LCMV infection, efficiently produced IFN-γ, and killed target cells (Figs. 1 and 2 and Figs. S1 and S2) (2, 12, 14, 17, 32, 36). The low-intensity calcium flux observed in CTL from KO mice likely is mediated, at least in part, by calcium channels other than CRAC, such as purigenic (P2X) and Ca_v1 channels that have been shown to support

T-cell proliferation (36, 37). The cytotoxicity mediated by CTL from KO mice was mediated by Fas/FasL and was highly efficient because of the increased FasL expression by CTL derived from KO mice (Fig. 1*F*). Consistent with this result is the observation that CTL from KO mice killed via Fas/FasL-mediated cytotoxicity in a Ca^{2+} independent, PI3K-dependent manner (Fig. 1) (28, 30, 39, 40).

FasL belongs to the TNF receptor family, which costimulates naive (e.g., CD27, CD28, CD40) and mature (e.g., 4.1BB and OX40) T cells (41–43). Thus it is conceivable that in CD8β-KO mice FasL provides costimulation to compensate for the impaired Ca^{2+}, NFAT signaling. Indeed, the cytoplasmic portion of FasL stably binds PI3K and MAP kinases, which together with PKCθ can signal T cells and thymocytes (30, 41–44). Moreover, the IFN-γ response of CTL from KO mice was strongly inhibited by the PI3K inhibitors Wortmannin and LY-294002 but not by CsA (Fig. 2*E*). Conversely, the IFN-γ response of CTL from WT mice was strongly reduced by CsA, and this result concurs with reports showing that IFN-γ signaling requires strong Ca^{2+} mobilization, calcineurin activation, and NFAT nuclear translocation (36, 38). The same was true for the cytolytic responses; that is, these CTL exhibited high Ca^{2+}- and NFAT-signaled perforin/granzyme-mediated cytotoxicity in addition to Ca^{2+}-independent, PI3K-signaled Fas/FasL-mediated killing.

D^b/GP33 tetramer binding was modestly more avid on CTL from KO mice (Fig. 2 *A* and *B*); larger differences were observed on CTL from B6, CD8β-KO, or CD8α-KO mice (2, 14), as is consistent with the view that CD8-independent CTL express high-affinity TCR (2, 14, 16). On the other hand, we observed marked binding differences for D^b/GP33- and CD8-binding–deficient $D^b_{226/227}$/GP33 tetramer on CTL from WT and B6 mice but not on CTL from KO and CD8βKO mice (Fig. 2 *A* and *B*) (2). Moreover, we have observed previously that CD8αβ strengthens pMHC monomer binding on cloned CTL to various degrees, depending on the TCR (19). Collectively these findings suggest that the contribution of CD8 to pMHC binding depends on the TCR sequence, i.e., on different TCR–pMHC docking modes, allowing different degrees of CD8 coengagement (23, 26, 27, 45). Although in our system all $CD8^+$ T cells expressed the P14 TCRβ chain, previous structural studies indicated that pMHC footprints on TCR can vary considerably, depending on the TRAV and CDR3α sequences (24, 45, 46, 47).

The TCR repertoires of preimmune $CD8^+$ T cells from WT and KO mice were remarkably diverse, and the frequencies of TRAV–TRAJ recombination depended on TRAV segment use (Fig. S3), as observed previously on $CD8^+$ T cells from preimmune B6 mice (22). Consistent with the widely held view that secondary TRAV–TRAJ rearrangement proceeds in a coordinated, sequential manner from proximal to more distant segments (21), recombination frequencies of the three most proximal TRAV genes decreased for distal TRAJ genes. However, for all other TRAV segments the observed recombination events were compatible with the view that secondary TRAV–TRAJ rearrangements rely on monoallelic, higher-order DNA looping that provides proximity of TRAV genes to RAG recombinase nested in TRAJ gene clusters (22, 48).

The TCR repertoires of D^b/GP33-specific CTL from LCMV-immune mice, especially from KO mice, were much less diverse than those of preimmune $CD8^+$ T cells (Fig. 3 and Fig. S5). Although the repertoires exhibited a substantial overlap, they also displayed distinct TRAV use; i.e., some TRAV segments were exclusively or preferentially found in one or the other repertoire (Fig. 4). The CDR1α and CDR2α sequences encoded by these TRAV segments exhibited different hydropathies and isoelectric points (Fig. 5 *A* and *B*). In canonical "diagonal" docking of TCR to pMHC, the CDR1α and CDR2α loops are poised to interact with the MHC α2 helix (23–27, 45). This canonical docking mode is imposed by the coreceptor CD8αβ, which, by coengaging TCR-associated pMHC, elicits CD3 phosphorylation by CD8-associated lck and thereby promotes thymic selection of $CD8^+$ T cells (1, 6, 45, 49). This signaling pathway is defective on $CD8\alpha\alpha^+$ T cells from CD8βKO mice (Figs. 1 and 2*E* and Fig. S2), and therefore CD8αα predictably infers little or no constraint on TCR–pMHC docking orientation, as is consistent with reports for coreceptor- and MHC-KO mice (49), for $CD8\alpha\alpha^+$ $TCR\gamma\delta^+$ T cells (50), and for $TCR\alpha\beta^+$ natural killer T cells (51). Numerous observations support the view that coreceptor dependence is contingent on TCR sequences and/or on the TCR–pMHC docking mode. (*i*) CTL from KO mice recognized GP33 peptide variants very differently than do CTL from WT mice (Fig. 1 *C–E*). (*ii*) Tetramer binding on CTL from WT, but not from KO, mice was substantially increased by CD8 coengagement (Fig. 2 *A* and *B*) (2). (*iii*) Structural analysis of a large number of TCR–pMHC complexes revealed noncanonical docking modes that did not allow significant Ca^{2+}, NFAT-dependent TCR signaling (23–27, 45, 49). (*iv*) TCR sequences have been shown to convey CD8 dependence (2, 14, 17–20). (*v*) The TCR of a CD8-independent CTL engaged its ligands in a noncanonical docking orientation (23).

About 16% of CTL from LCMV-immune WT mice were CD8 independent; i.e., their IFN-γ response was not affected by CD8 blocking, by mutations ablating CD8 binding in the MHC α3 domain, or by the inhibition of calcineurin and NFAT by CsA (Figs. 5 *D* and *E*). Although the TCR repertoire of the CD8-independent CTL from KO mice was narrower than that from WT mice, it contained sequences that were not or were infrequently expressed on the CTL from WT mice (Figs. 3 and 4 and Fig. S6). We speculate that these TCR may engage pMHC in noncanonical configurations that do not favor efficient CD8 coengagement and Ca^{2+}- and NFAT-dependent TCR signaling but permit signaling via a Ca^{2+}-independent, PI3K-dependent pathway (Fig. 5*C*). Disruption of the CD8β gene resulted in ablation of the dominant Ca^{2+}- and NFAT-dependent signaling pathway, forcing $CD8^+$ T cells to signal via this alternative pathway. We hypothesize that T cells that lack CD8β (e.g., natural killer T cells, γδ T cells, or intraepithelial lymphocytes), as well as a minor fraction of $CD8\alpha\beta^+$ T cells that are CD8 independent for structural reasons, signal via this other pathway. Because TCR–pMHC docking modes cannot be deduced from TCR sequences, this conclusion is speculative. This duality of the CD8 compartment may provide organisms with a better chance of overcoming cancer or infections by providing a second response when the first compartment fails to contain the threat (52).

Materials and Methods

Mice and Infection. KO mice were generated by crossing P14 TCRβ-chain transgenic mice (53) with CD8βKO mice (13). Mice (7- to 10-wk-old) were injected i.v. with 200 pfu of LCVM strain Armstrong (2). The $CD8^+$ T cells from spleens of naive or LCMV-infected mice (8 d postinfection) were isolated using negative MACS selection (Miltenyi Biotec). All protocols were approved by the Cantonal Veterinary Office (Lausanne, Switzerland).

Tetramers and Antibodies. Splenocyte were stained in FACS buffer (PBS with 1% BSA and 0.01% sodium azide) with 10 nM of D^b/GP33 tetramers (from TCMetrix) for 30 min at 4 °C, followed by staining with anti-CD8α or anti-CD4 antibody. Antibodies specific for CD4 (clone GK1.5), CD8α (53.6.7), CD5 (53.7), CD25 (PC61), CD44 (IM.781), CD62L (Mel14), or CD127 (A7R34) were conjugated with FITC and purified using standard protocols or with phycoerythrin using a conjugation kit from Europa BioProducts. Antibodies specific for IFN-γ, TNF-α, and CD107a were from eBioscience and anti-FasL blocking antibody (MFL3) was obtained from BioLegend. For tetramer-binding studies $CD8\alpha^+$ T cells were isolated from splenocytes by negative selection using the $CD8\alpha^+$ T-cell isolation kit II from Miltenyi.

Intracellular Staining. Splenocytes were incubated for 4–6 h in 96-well plates with 1/1,000 GolgiStop (BD Biosciences) and the indicated concentration of GP33 peptides. Cells then were permeabilized with Cytofix/Cytoperm solution and stained with anti–IFN-γ, TNF-α, or FasL antibodies according to the manufacturer's instructions (BD Biosciences). In some experiments the cells were preincubated with Wortmannin (0.1 μM), LY294002 (50 μM), or CsA (0.1 μM) for 30 min; the drugs treatment was maintained during the stimulation process.

Cytotoxic Assay. ^{51}Cr-labeled D^b-transfected P815 cells (5×10^3 cells per well) (2) were incubated for 30 min at 37 °C with the indicated concentrations of GP33

peptides and then were incubated with CD8$^+$ T cells at an effector/target ratio of 10/1. After 6 h of incubation at 37 °C, the specific lysis was calculated from the released ^{51}Cr as previously described (2). In some experiments, cells were pretreated for 30 min with FasL-blocking antibody (50 ng/mL) or CMA (100 nM); FasL-blocking antibody and CMA were maintained during the assay. For CD107a assay, CD8$^+$ CTL were incubated for 6 h with the indicated concentration of GP33 peptide, GolgiStop (1/1,000) (BD Biosciences), and anti-CD107a antibody. After incubation the cells were stained with D^b/GP33 tetramer and analyzed by flow cytometer on a LSR II instrument (BD Biosciences).

Calcium Mobilization. P815/D^b cells were left unpulsed or were pulsed with 1 μM of GP33 peptide for 1 h at 37 °C in serum-free DMEM. Purified CTL (1×10^6 cells/mL) were incubated with 2 μM Indo-1/AM (Sigma) for 45 min at 37 °C in serum-free cDMEM. After washing, CTL were resuspended at 1×10^6 cells/mL in serum-free cDMEM and mixed with target cells (E/T = 1/3), sedimented by centrifugation (1 min, 300 × *g*), and suspended, and calcium-dependent Indo-1 fluorescence was measured by flow cytometry for 5 min of incubation at 37 °C, essentially as described (9).

TCR Sequence Analysis. Sequencing of the TCRα chain transcripts and sequence analysis were performed as previously described (22). Briefly, total RNA was extracted from naive CD8$^+$ T cells or from D^b/GP33 tetramer-sorted CD8$^+$ T cells. TCRα chain mRNA was amplified by in vitro transcription and sequenced using Illumina technology, The data were analyzed using ad hoc Perl scripts. Out-of-frame sequences and singletons were excluded from the analysis.

ACKNOWLEDGMENTS. We thank Dr. A. Wilson and D. Labes for support with flow cytometry and sorting and Drs. Rob MacDonald and Dan Littman for providing the P14β transgene and CD8βKO mice. This work was supported Swiss National Science Foundation Grant 310030_12533/1.

1. Starr TK, Jameson SC, Hogquist KA (2003) Positive and negative selection of T cells. *Annu Rev Immunol* 21(1):139–176.
2. Angelov GS, Guillaume P, Luescher IF (2009) CD8beta knockout mice mount normal anti-viral CD8+ T cell responses—but why? *Int Immunol* 21(2):123–135.
3. Arcaro A, et al. (2001) CD8beta endows CD8 with efficient coreceptor function by coupling T cell receptor/CD3 to raft-associated CD8/p56(lck) complexes. *J Exp Med* 194(10): 1485–1495.
4. Doucey MA, et al. (2001) CTL activation is induced by cross-linking of TCR/MHC-peptide-CD8/p56lck adducts in rafts. *Eur J Immunol* 31(5):1561–1570.
5. Bosselut R, et al. (2000) Role of CD8beta domains in CD8 coreceptor function: Importance for MHC I binding, signaling, and positive selection of CD8+ T cells in the thymus. *Immunity* 12(4):409–418.
6. Singer A, Adoro S, Park JH (2008) Lineage fate and intense debate: Myths, models and mechanisms of CD4- versus CD8-lineage choice. *Nat Rev Immunol* 8(10):788–801.
7. Cheroutre H, Lambolez F (2008) Doubting the TCR coreceptor function of CD8alphaalpha. *Immunity* 28(2):149–159.
8. Wang R, Natarajan K, Margulies DH (2009) Structural basis of the CD8 alpha beta/MHC class I interaction: Focused recognition orients CD8 beta to a T cell proximal position. *J Immunol* 183(4):2554–2564.
9. Doucey MA, et al. (2003) CD3 delta establishes a functional link between the T cell receptor and CD8. *J Biol Chem* 278(5):3257–3264.
10. Renard V, Romero P, Vivier E, Malissen B, Luescher IF (1996) CD8 beta increases CD8 coreceptor function and participation in TCR-ligand binding. *J Exp Med* 184(6):2439–2444.
11. Wang X, et al. (2008) Dynamics of proximal signaling events after TCR/CD8-mediated induction of proliferation or apoptosis in mature CD8+ T cells. *J Immunol* 180(10): 6703–6712.
12. Fung-Leung WP, et al. (1994) Reduced thymic maturation but normal effector function of CD8+ T cells in CD8 beta gene-targeted mice. *J Exp Med* 180(3):959–967.
13. Crooks ME, Littman DR (1994) Disruption of T lymphocyte positive and negative selection in mice lacking the CD8 beta chain. *Immunity* 1(4):277–285.
14. Riddle DS, et al. (2008) Rescue of cytotoxic function in the CD8alpha knockout mouse by removal of MHC class II. *Eur J Immunol* 38(6):1511–1521.
15. Goldrath AW, Hogquist KA, Bevan MJ (1997) CD8 lineage commitment in the absence of CD8. *Immunity* 6(5):633–642.
16. Kerry SE, et al. (2003) Interplay between TCR affinity and necessity of coreceptor ligation: High-affinity peptide-MHC/TCR interaction overcomes lack of CD8 engagement. *J Immunol* 171(9):4493–4503.
17. Andrews NP, Pack CD, Lukacher AE (2008) Generation of antiviral major histocompatibility complex class I-restricted T cells in the absence of CD8 coreceptors. *J Virol* 82(10): 4697–4705.
18. McNicol AM, et al. (2007) CD8alpha/alpha homodimers fail to function as co-receptor for a CD8-dependent TCR. *Eur J Immunol* 37(6):1634–1641.
19. Kessler BM, Bassanini P, Cerottini JC, Luescher IF (1997) Effects of epitope modification on T cell receptor-ligand binding and antigen recognition by seven H-2Kd-restricted cytotoxic T lymphocyte clones specific for a photoreactive peptide derivative. *J Exp Med* 185(4):629–640.
20. Auphan N, et al. (1994) The degree of CD8 dependence of cytolytic T cell precursors is determined by the nature of the T cell receptor (TCR) and influences negative selection in TCR-transgenic mice. *Eur J Immunol* 24(7):1572–1577.
21. Shih HY, Hao B, Krangel MS (2011) Orchestrating T-cell receptor α gene assembly through changes in chromatin structure and organization. *Immunol Res* 49(1-3):192–201.
22. Genolet R, Stevenson BJ, Farinelli L, Osterås M, Luescher IF (2012) Highly diverse TCRα chain repertoire of pre-immune CD8$^+$ T cells reveals new insights in gene recombination. *EMBO J* 31(7):1666–1678.
23. Buslepp J, Wang H, Biddison WE, Appella E, Collins EJ (2003) A correlation between TCR Valpha docking on MHC and CD8 dependence: Implications for T cell selection. *Immunity* 19(4):595–606.
24. Adams JJ, et al. (2011) T cell receptor signaling is limited by docking geometry to peptide-major histocompatibility complex. *Immunity* 35(5):681–693.
25. Gras S, et al. (2012) A structural voyage toward an understanding of the MHC-I-restricted immune response: Lessons learned and much to be learned. *Immunol Rev* 250 (1):61–81.
26. Wang JH, Reinherz EL (2012) The structural basis of αβ T-lineage immune recognition: TCR docking topologies, mechanotransduction, and co-receptor function. *Immunol Rev* 250(1):102–119.
27. Cole DK, et al. (2012) The molecular determinants of CD8 co-receptor function. *Immunology* 137(2):139–148.
28. Kassahn D, et al. (2009) Distinct requirements for activation-induced cell surface expression of preformed Fas/CD95 ligand and cytolytic granule markers in T cells. *Cell Death Differ* 16(1):115–124.
29. Pores-Fernando AT, Zweifach A (2009) Calcium influx and signaling in cytotoxic T-lymphocyte lytic granule exocytosis. *Immunol Rev* 231(1):160–173.
30. Pardo J, et al. (2003) Differential implication of protein kinase C isoforms in cytotoxic T lymphocyte degranulation and TCR-induced Fas ligand expression. *Int Immunol* 15(12):1441–1450.
31. Kataoka T, et al. (1996) Concanamycin A, a powerful tool for characterization and estimation of contribution of perforin- and Fas-based lytic pathways in cell-mediated cytotoxicity. *J Immunol* 156(10):3678–3686.
32. Liu JO (2009) Calmodulin-dependent phosphatase, kinases, and transcriptional corepressors involved in T-cell activation. *Immunol Rev* 228(1):184–198.
33. Stadinski BD, et al. (2011) A role for differential variable gene pairing in creating T cell receptors specific for unique major histocompatibility ligands. *Immunity* 35(5):694–704.
34. Dash P, et al. (2011) Paired analysis of TCRα and TCRβ chains at the single-cell level in mice. *J Clin Invest* 121(1):288–295.
35. Hopp TP, Woods KR (1981) Prediction of protein antigenic determinants from amino acid sequences. *Proc Natl Acad Sci USA* 78(6):3824–3828.
36. Oh-hora M (2009) Calcium signaling in the development and function of T-lineage cells. *Immunol Rev* 231(1):210–224.
37. Badou A, Jha MK, Matza D, Flavell RA (2013) Emerging roles of L-type voltage-gated and other calcium channels in T lymphocytes. *Front Immunol* 4(30):243.
38. Teixeira LK, et al. (2005) IFN-gamma production by CD8+ T cells depends on NFAT1 transcription factor and regulates Th differentiation. *J Immunol* 175(9):5931–5939.
39. Guillaume P, et al. (2003) Soluble major histocompatibility complex-peptide octamers with impaired CD8 binding selectively induce Fas-dependent apoptosis. *J Biol Chem* 278(7):4500–4509.
40. Kessler B, et al. (1998) Peptide modification or blocking of CD8, resulting in weak TCR signaling, can activate CTL for Fas- but not perforin-dependent cytotoxicity or cytokine production. *J Immunol* 161(12):6939–6946.
41. So T, Croft M (2013) Regulation of PI-3-Kinase and Akt Signaling in T Lymphocytes and Other Cells by TNFR Family Molecules. *Front Immunol* 139(4):1–11.
42. Sun M, Ames KT, Suzuki I, Fink PJ (2006) The cytoplasmic domain of Fas ligand costimulates TCR signals. *J Immunol* 177(3):1481–1491.
43. Sun M, et al. (2007) Cutting edge: Two distinct motifs within the Fas ligand tail regulate Fas ligand-mediated costimulation. *J Immunol* 179(9):5639–5643.
44. Gruber T, Pfeifhofer-Obermair C, Baier G (2010) PKCtheta is necessary for efficient activation of NFkappaB, NFAT, and AP-1 during positive selection of thymocytes. *Immunol Lett* 132(1-2):6–11.
45. Garcia KC (2012) Reconciling views on T cell receptor germline bias for MHC. *Trends Immunol* 33(9):429–436.
46. Deng L, Langley RJ, Wang Q, Topalian SL, Mariuzza RA (2012) Structural insights into the editing of germ-line-encoded interactions between T-cell receptor and MHC class II by Vα CDR3. *Proc Natl Acad Sci USA* 109(37):14960–14965.
47. Birnbaum ME, Dong S, Garcia KC (2012) Diversity-oriented approaches for interrogating T-cell receptor repertoire, ligand recognition, and function. *Immunol Rev* 250(1):82–101.
48. Chaumeil J, et al. (2013) Higher-order looping and nuclear organization of Tcra facilitate targeted rag cleavage and regulated rearrangement in recombination centers. *Cell Rep* 3(2):359–370.
49. Van Laethem F, Tikhonova AN, Singer A (2012) MHC restriction is imposed on a diverse T cell receptor repertoire by CD4 and CD8 co-receptors during thymic selection. *Trends Immunol* 33(9):437–441.
50. Adams EJ, Chien YH, Garcia KC (2005) Structure of a gammadelta T cell receptor in complex with the nonclassical MHC T22. *Science* 308(5719):227–231.
51. Pellicci DG, et al. (2009) Differential recognition of CD1d-alpha-galactosyl ceramide by the V beta 8.2 and V beta 7 semi-invariant NKT T cell receptors. *Immunity* 31(1):47–59.
52. Meiraz A, Garber OG, Harari S, Hassin D, Berke G (2009) Switch from perforin-expressing to perforin-deficient CD8(+) T cells accounts for two distinct types of effector cytotoxic T lymphocytes in vivo. *Immunology* 128(1):69–82.
53. Brändle D, et al. (1991) Involvement of both T cell receptor V alpha and V beta variable region domains and alpha chain junctional region in viral antigen recognition. *Eur J Immunol* 21(9):2195–2202.